Exploring electrohydrodynamic flows inside leaky dielectric drops: a laser velocimetry approach

Joel Karp, Franck Lefebvre, G. Godard, Saïd Idlahcen, Bertrand Lecordier, Mostafa Safdari Shadloo

Exploring electrohydrodynamic flows inside leaky dielectric drops: a laser velocimetry approach

J. R. Karp[1], F. Lefebvre[1], G. Godard[1], S. Idlahcen[1], B. Lecordier[1], M. S. Shadloo[1, 2, *]

1: INSA Rouen Normandie, Univ Rouen Normandie, CNRS, Normandie Univ, CORIA UMR 6614, F-76000 Rouen, France
2: Institut Universitaire de France, Rue Descartes, F-75231 Paris, France
* Correspondent author: msshadloo@coria.fr

Keywords: Electrohydrodynamics, Lagrangian Particle Tracking (LPT), leaky dielectric model (LDM)

ABSTRACT

A novel experimental methodology based on laser velocimetry for the investigation of electrohydrodynamic (EHD) flows inside a neutrally buoyant leaky dielectric drop of 2.25 mm of radius is proposed. Utilizing fluorescent particles, 2D and 3D Lagrangian Particle Tracking (LPT) measurements of the EHD flows inside an initially spherical drop under a constant electric field are reported. Two leaky dielectric fluids, namely Silicone and Castor oils, were used as either the drop or the medium phases, depending on the case investigated, thus covering oblate and prolate drops both with small and larger deformations. 2D measurements of the trajectories and velocities of the tracer particles in a Lagrangian referential enabled a direct comparison with the leaky dielectric model (LDM), a well-stablished theory covering drops with smaller deformations, showing a good agreement with our measurements. The symmetry inside a drop with increased deformation is investigated from an analysis of the mean 3D velocity field, whose measurements converge to the two-dimensional analysis at the plane of symmetry of the drop, suggesting symmetrical flow structures inside the drop.

1. Introduction

Electrohydrodynamic (EHD) flows are generated by electric stresses shearing at fluid interfaces (Vlahovska, 2019); they are relevant in the energy sector, pharmaceutical industry, as well as medical applications (Karp *et al.*, 2024; Mikkelsen *et al.*, 2018). For the particular case of a neutrally buoyant drop under a constant electric field, as shown in Fig. 1 (a), an analytical solution known as the leaky dielectric model (LDM) has been proposed by Taylor (1966) to obtain the velocity field inside the drop:

$$\hat{u}_r = \left[\left(\frac{r}{a_o}\right)^3 - \left(\frac{r}{a_o}\right)\right] U_m(1 - 3\cos^2\theta) \quad (1)$$

$$\hat{u}_\theta = \frac{1}{2}\left[5\left(\frac{r}{a_o}\right)^3 - 3\left(\frac{r}{a_o}\right)\right] U_m \sin 2\theta \quad (2)$$

where $\hat{u}_r$ and $\hat{u}_\theta$ are the radial and tangential velocity components, respectively. a_0 is the initial radius of the drop and $U_m = (9\epsilon E_o^2 R(S-R))/[10\mu(1+\hat{\mu}/\mu)(R+2)^2]$ is the maximum velocity. This set of equations consider a spherical drop dispersed in a liquid with same density ρ, but different viscosities ($\hat{\mu}$ and μ), electrical conductivities ($\hat{\sigma}$ and σ) and permitivities ($\hat{\epsilon}$ and ϵ), where the hat symbol denotes a quantity associated to the drop phase. $R = \hat{\sigma}/\sigma$ and $S = \hat{\epsilon}/\epsilon$ are the conductivity and permittivity ratios, respectively. The model considers both fluids to be leaky dielectric, $i.e.$, with small electric conductivities under a relatively weak electric field, a condition known as the small-deformation limit, $Ca_E \ll 1$, where $Ca_E = \epsilon E_o^2 a_o/\gamma$ is the electric capillary number (Saville, 2003).

Experimental investigations of the shape of drops under a direct electric field were reported, obtaining a good agreement with the LDM predictions within the small-deformation limit (Torza & Mason, 1971). Nevertheless, the need for adjustments have been pointed out for drops with larger deformations for which the assumptions considered are no longer valid. Moreover, such verifications are mostly based on high-speed shadowgraph images of the contour of the drop, whose deformation is the parameter used for comparison. Measurements of the velocity field have been reported for the first time by Karp *et al.* (2024), who proposed a critical value for the capillary number of $Ca_E \approx 0.1$ below which the LDM model describes well the internal circulation, based on profiles of the radial and tangential velocity components inside the drop. However, additional experimental measurements are then required to address this issue, particularly towards the three-dimensional evaluation of drop EHD flows, measurements that to the best of our knowledge have not been reported to date. From an optical diagnostic point of view, the measurements of the internal EHD flows of a drop are challenging owing to the small dimensions of the flow structures and also the differences in the optical indexes. In this paper, we propose a methodology based on both two-dimensional and three-dimensional Lagrangian Particle Tracking (LPT) using fluorescent particles to address this problem.

2. Experimental methods

Two-dimensional measurements

The experiments were performed in cuvette made of plexiglass completely filled with a stagnant leaky dielectric liquid, as shown in Fig. 1 (b), in which two vertical copper electrodes (1 mm thickness) are placed 20 mm apart. The electric field is generated using a high-voltage supply system to apply the desired voltage. A drop of fixed size ($a_o = 2.25$ mm for cases I and II and

$a_o = 4.0$ mm for case III) is introduced using a micropipette. Silicone and Castor oils are used in this study as the leaky dielectric liquids, whose properties are listed in Tab. 1. One of the main features of the LDM theory is that the consideration of leaky dielectric liquids allows the existence of a tangential component of the electric stresses at the interface, thus changing the sense of the fluid circulation shown in Fig. 1 (a) when the system of fluids is reversed. Therefore, two cases are investigated here, as shown in Tab. 2. The Silicone and Castor oils serve as either the drop or the continuous phase, leading to two shape configurations: the oblate and prolate, in which the major axis of the drop is perpendicular and parallel to the direction of the electric field, respectively. The strength of the electric field E_o is adapted to each case so that we remain within the small-deformation limit for cases I and II, whereas a more deformed drop is considered for case III.

Table 1: Properties of the leaky dielectric liquids used in this study. The interfacial tension is $\gamma = 4$ mN/m.

	Density, ρ (kg/m^3)	Viscosity, μ (Pa.s)	Electrical permitivitty, ϵ (F/m)	Electrical conductivity, σ (S/m)	Refractive index, n
Silicone oil	970	0.50	28.3	0.87	1.42
Castor oil	961	0.78	41.6	30.1	1.45

Table 2: Cases analyzed in this study, indicating the fluids serving as the drop and the medium and the strength of the electric field (E_o). The table also presents permittivity ratio (S) and the conductivity ratio (R) and the shape adopted by the drop.

Case	Fluid		E_o	$S = \hat{\epsilon}/\epsilon$	$R = \hat{\sigma}/\sigma$	Ca_E	Shape
	Drop	Medium	(kV/cm)				
I	Castor oil	Silicone oil	0.30	1.47	34.48	0.012	Oblate
II	Silicone oil	Castor oil	0.50	0.68	0.029	0.060	Prolate
III			0.75			0.27	

The EHD flows were quantified by adding RhodamineB tracer particles (20 μm) in the drop phase and illuminating the drop at its plane of symmetry with a laser sheet (roughly 150 μm thick), as shown in Fig. 1 (b). A monocavity Nd:YAG laser (Quantel BRIO SP23, France) of 64 mJ and 532 nm served as the laser source. A CCD camera (CX3-25, LaVision, Germany) with a resolution of 5296 x 4584 pixels and 12 bits of digital output, coupled to a 105 mm lens (Nikkon Makro, Japan) with an additional extension ring of 32 mm captured time-resolved images with an acquisition rate of 20 Hz. Using the same set-up, with the addition of a LED back-source illumination, shadowgraph images were also obtained to visualize time evolution of the contour of the drop under the electric field.

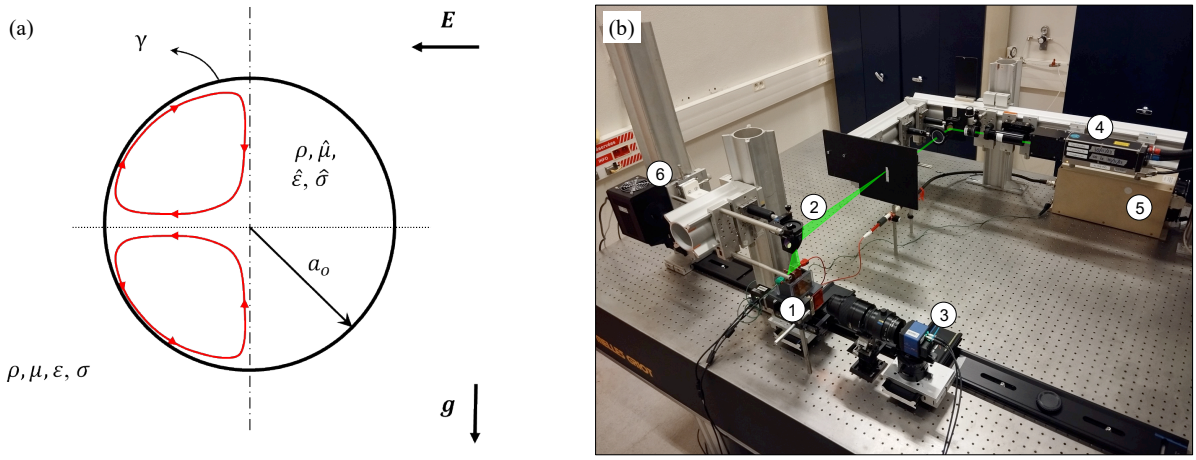

Figure 1: (a) Illustration of the fluid system showing the electric and gravitational fields and the properties of the fluids. (b) Experimental apparatus for measuring the two-dimensional internal EHD flows of the drop showing the cuvette (1), laser sheet (2), CCD camera (3), laser source (4), high-voltage power supply (5), and backlight illumination source (6).

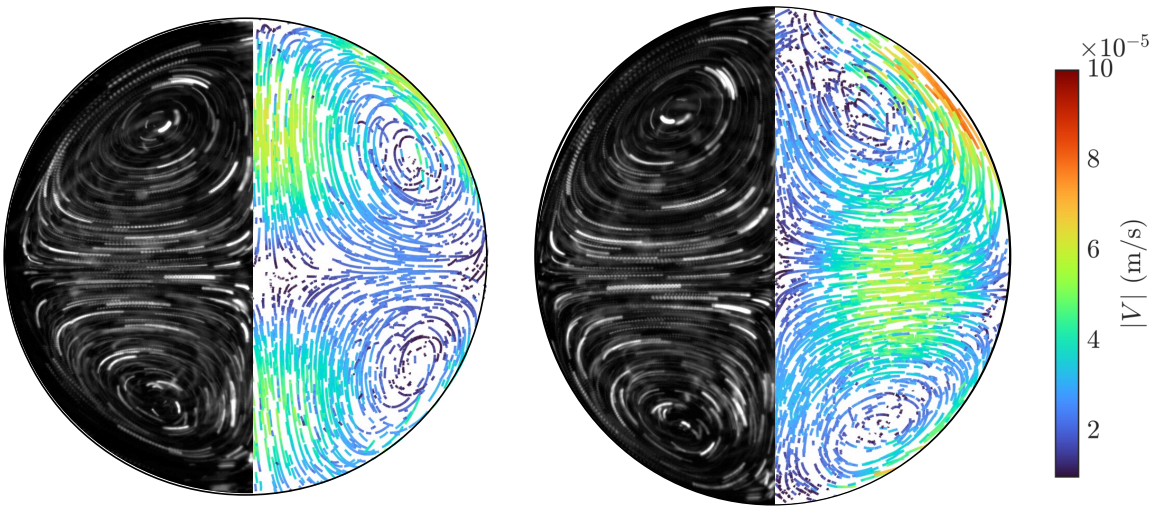

Figure 2: Sample images displaying the results obtained for the velocity field in Lagrangian referential for cases I (left) and II (right). The images show the streaklines of the tracer particles (left halves of each sub-figure) and the trajectories obtained using the LPT method (right halves of each subfigure).

The LPT method was employed to measure the circulation within the droplet. The relatively low concentration of seeding particles facilitated the quantification of the velocity field within a Lagrangian reference frame, thereby enhancing spatial resolution. An in-house Python code was written to track each particle using the histogram matching method, employing a triangulation iterative process for estimating the most probable particle position. The minimum size of the particle is set to 6 pixels and a minimum intensity of 500 is considered. The field of search for the tracking method is set to 10 pixels, approximately twice the maximum particle displacement. The

time-resolved particle tracking algorithm was performed over a series of 50 sequential frames. Figure 2 shows sample images of the trajectories of the tracer particles and their velocities in a Lagrangian referential for both cases investigated. Streaklines obtained by summing the intensity of each pixel over the whole sequence of images (displayed on the left halves of each subfigure) provide a qualitative overview of the vortical structures present inside the drop, while a quantitative representation is shown on the right halves of each subfigure.

Three-dimensional measurements

The LDM theory covers only the two-dimensional dimensional flow at the plane of symmetry of the drop, which offers enough information for the cases with small deformations in which the symmetry of the circulation is maintained. Three-dimensional measurements are however required for more deformed drops, for which a symmetry breakup is frequently reported [4]. Although some attempts from previous researchers [1], a closed-form solution of the 3D velocity field inside the drop is very difficult under those conditions due to the non-linearity of the transport equations. We propose to extend the aforementioned methodology to allow three-dimensional measurements of the particle tracking by a multiple camera arrangement. Due to the restricted optical access of the chamber, we opted for an optical arrangement with three cameras placed in line, as shown in Fig. 3. The cameras (HiSense Zyla, Dantec, Danemark) also employ a CCD sensor with a spatial resolution of 2560 x 2160 pixels and a 12 bits digital output. The additional parts of the optical system are the same as for the 2D measurements. The Scheimpflug principle is used here to correct the effect of the inclination of the cameras. When a lens is tilted with respect to the camera sensor, an extended tangent line originating from the sensor plane and one from the lens meet at a line through which the plane of focus passes. By doing so, a proper focus of the tracer particles can be obtained for the whole drop. As can be seen in Fig. 3, the distance between the object and the optical arrangement is increased for the three-dimensional measurements, leading to a larger field of view of roughly 16 x 16 mm for each camera. The calculation of the Scheimpflug angle for the tilt of the lens depends mostly on the distance of the object to the sensor plane and the enlargement factor of the object. The angle is set at around 20° in order to be able to place the drop as close as possible to the camera arrangement. Note that due to the increased distance between the drop and the sensors for the multiple cameras in the in-line configuration, the size of the drop was increased up to $a_o = 4$ mm for the sake of visualization.

The reconstruction of the three-dimensional velocity fields requires a volumetric calibration performed from the images obtained by each camera. A dotted target with known point

dimensions (0.5 mm for the dot diameter and 2 mm spacing) is used for this matter. The calibration target is recorded simultaneously by each camera, for different positions (-5 mm to 5 mm) along the *z*-direction. Then, once the positions of the calibration target are known and the images with the known image points from the target are acquired, a mathematical procedure is undertaken to recreate the 3D coordinates based on the 2D coordinates visualized on the camera images. Such a procedure generates a camera model with the reconstructed coordinates and, in this paper, is based on the polynomial method to take the optical distortions into account. In this calibration procedure, special care was taken to obtain a proper alignment and accuracy of the position of the calibration target to ensure a well-defined transformation for the 2D to 3D coordinates. Before applying the reconstruction of the particle field in a volume in space, a 3D self-calibration procedure (LaVision Davis V10) is performed from images of tracer particles filling the entire volume of the tank. The characteristic value for reconstruction accuracy in the drop region is of the order of 0.25 voxel after calibration refinement.

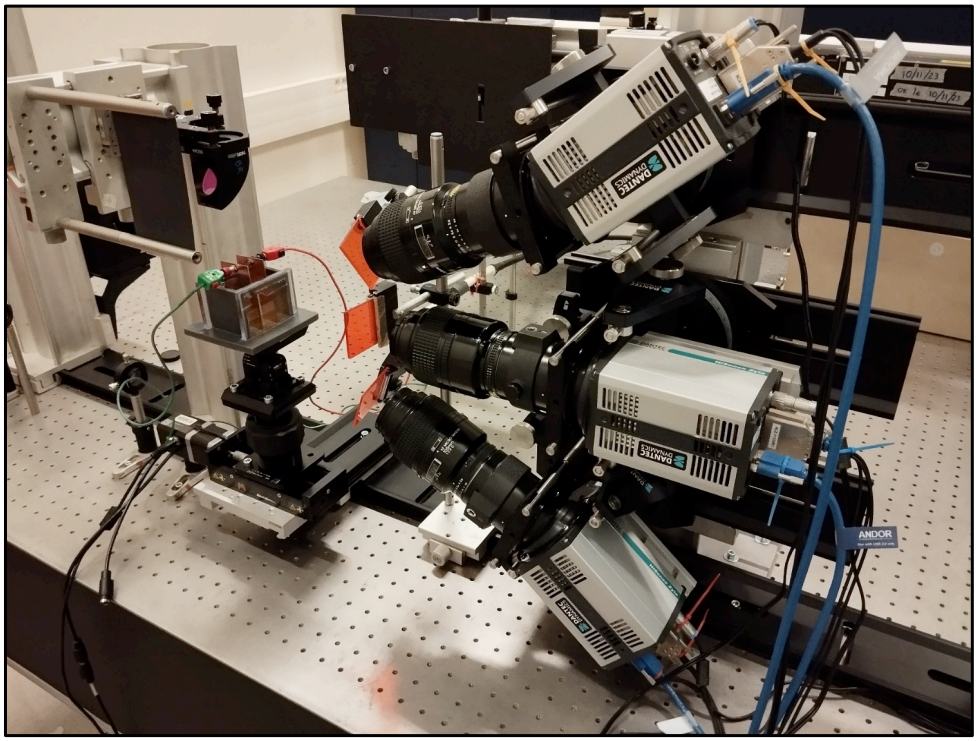

Figure 3: Experimental apparatus for measuring the three-dimensional internal EHD flows of the drop.

The three-dimensional positions of the particles can be obtained from the raw images using the Shake-the-Box method (STB). This algorithm begins with an initial guess of the particle positions using standard Lagrangian techniques. Firstly, these two-dimensional locations are obtained by identifying the particles centroids, whose locations are then projected along their epipolar lines

in to the other cameras. Statistical procedures are used to estimate the most probable three-dimensional particle locations based on the 2D projections along the epipolar line. Then, the STB method iteratively perturbs the predicted position in the 3D space to find the best matching location of the particle.

3. Results

Shape deformation

We begin our analysis by showing the shape contours of the drops for cases I and II to confirm whether the small-deformation limit can be considered for cases I and II. Figure 5 shows steady-state images of the drops without electric field with the same fluids systems for cases I and II, as shown in Fig. 5 (a) and (c), respectively, for which a spherical shape is identified. Once an electric is applied to the drops, according to the cases listed in Tab. 2, the drop either deforms into an oblate or prolate configuration, as shown in Fig. 5 (b) and (d), respectively. The deformation parameter of the drop is calculated as $D = (L - W)/(L + W)$, where L and W are the drop axes parallel and perpendicular to the drop, respectively. As we clearly remain within the small-deformation limit given that $Ca_E \ll 1$ for both cases investigated here (see the values shown in Tab. 2), the drops retain their nearly spherical shape under the electric field. The values of the deformation parameter D are -0.0115 for case I and 0.0122 for case II. Note that the negative value of D for case I is inherent to its oblate shape.

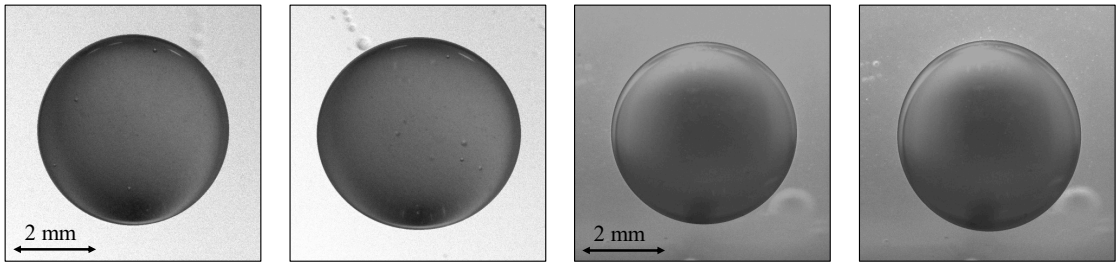

Figure 5: Spherical shape of the drop without electric field for the same fluid systems of cases I (a) and II (c). Deformed shape of the drop for cases I (b) and II (d).

Two-dimensional velocity field

Given that the condition for the small-deformation theory is valid for both cases investigated, next we can analyze the velocity field inside the drop. However, the particle trajectories and velocities shown in Fig. 2 are obtained in a Lagrangian referential and therefore its comparison with the

analytical solution expressed by Eqs. (1) and (2) is not straightforward and a conversion to a Eulerian referential is required. First, the local fluid deformation is quantified by computing the deformation gradient F, which is a matrix representation of the partial derivatives of fluid velocities with respect to spatial coordinates:

$$F = \begin{bmatrix} \frac{\partial \hat{u}_r}{\partial r} & \frac{1}{r}\frac{\partial \hat{u}_r}{\partial \theta} - \frac{\hat{u}_\theta}{r} \\ \frac{\partial \hat{u}_\theta}{\partial r} & \frac{1}{r}\frac{\partial \hat{u}_\theta}{\partial \theta} - \frac{\hat{u}_r}{r} \end{bmatrix}$$

The conversion of Lagrangian velocities to Eulerian velocities is then accomplished using the relationship:

$$\langle \frac{\hat{u}_r}{\hat{u}_\theta} \rangle_{Eulerian} = F \cdot \langle \frac{\hat{u}_r}{\hat{u}_\theta} \rangle_{Lagrangian}$$

Figure 5 shows radial profiles of the experimental values of the radial velocity component obtained with the aforementioned methodology for both cases analyzed. The radial profiles are shown for three values of the azimuthal angle $\theta = 0$, $\theta = \pi/4$, and $\theta = \pi/2$ that correspond to the horizontal, diagonal, and vertical lines in a Cartesian system of units. Note that the measurements of only one quadrant of the velocity field shown in Fig. 2 is displayed here. The radial component of the velocity is greater in the vertical and horizontal directions for cases I and II, respectively, suggesting that the circulation inside the drop is from the poles to the equator (case I) and from the equator to the poles (case II).

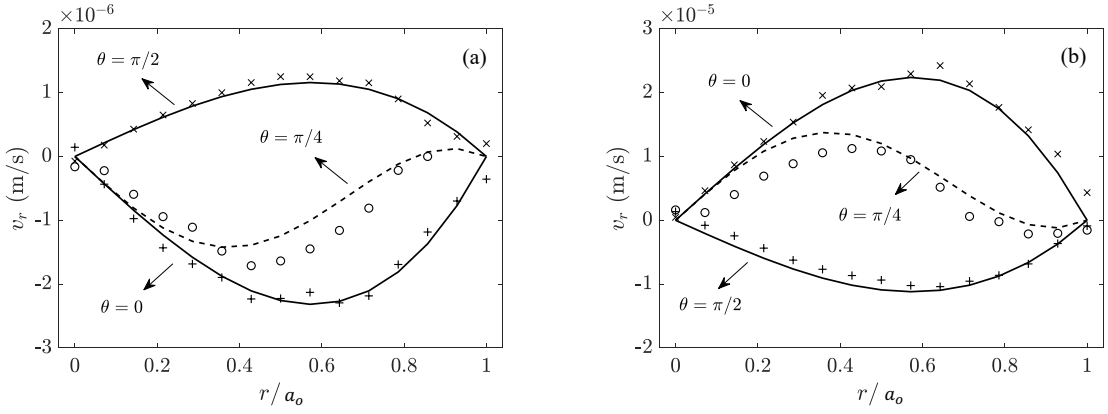

Figure 5: Radial profiles of the radial component of the velocity, v_r, for cases I (a) and II (b). The radial profiles are shown for three values of the azimuthal angle: $\theta = 0$, $\theta = \pi/4$, and $\theta = \pi/2$, that correspond to the horizontal, diagonal, and vertical lines, respectively. Markers indicate the experimental measurements and the lines refer to the analytical solution.

A direct comparison with the analytical predictions (black lines in Fig. (5)) of the radial velocity component given by Eqs. (1) and (2) show an excellent agreement of our measurements with the LDM theory. Considering the profiles at the axes of symmetry of the drop, $i.e.$, $\theta = 0$ and $\theta = \pi/2$,

a parabolic behavior (slightly inclined toward the region where $r/a_o \rightarrow 1$) is present for both cases analyzed. At $\theta = \pi/4$, the velocity oscillates due to the presence of an additional stagnation point, located at the center of the vortex inside the drop, roughly at $r/a_o = 0.7$.

Three-dimensional velocity field

Similar to the two-dimensional analysis, the 3D velocity field is obtained in a Lagrangian referential. Although this offers advantages in the calculation, the exploitation of the data is less trivial. Therefore, a conversion to a regular Eulerian grid is also performed here using the inverse distance interpolation. The field variable φ_E at a specific Eulerian point is estimated based on the values at nearby Lagrangian points. The distance from the Eulerian point to each nearby Lagrangian point d_i is used to calculate the weight parameter $w_i = 1/d_i^2$ which then leads to a normalized weight $W_i = w_i/\sum_j w_j$ where j is the number of Eulerian-based points. φ_E is then obtained based on the field variable at each Lagrangian point φ_i with $\varphi_E = \sum_i w_i \varphi_i$. The interpolation is performed over a sequence of 250 images, given that the flow is at permanent regime.

By using this method, the mean velocity vectors on a regular Eulerian grid can be obtained, as shown in Fig. 6. Note that case III is considered here, for which the small-deformation limit is no longer applicable. The goal to do so is to highlight the asymmetry of the flow circulation inside the drop for a more deformed configuration. The figure clearly depicts the three-dimensional structure of the vortical structures present inside the drop. Note that for visualization purposes, 2D slices are shown at $x/a_o = y/a_o = z/a_o = 0$ with the dimensionless positions ranging from 0 to 1 in each direction. The velocity field clearly indicates the presence of two counter-rotating vortical structures in this region of the drop. Near the interface of the drop, a stronger tangential component is observed. Therefore, a visual inspection of Fig. 6 suggests a strong similarity with the 2D results at $z/a_o = 0$, where the flow structure resembles the one obtained by the 2D methodology, despite its increased deformation.

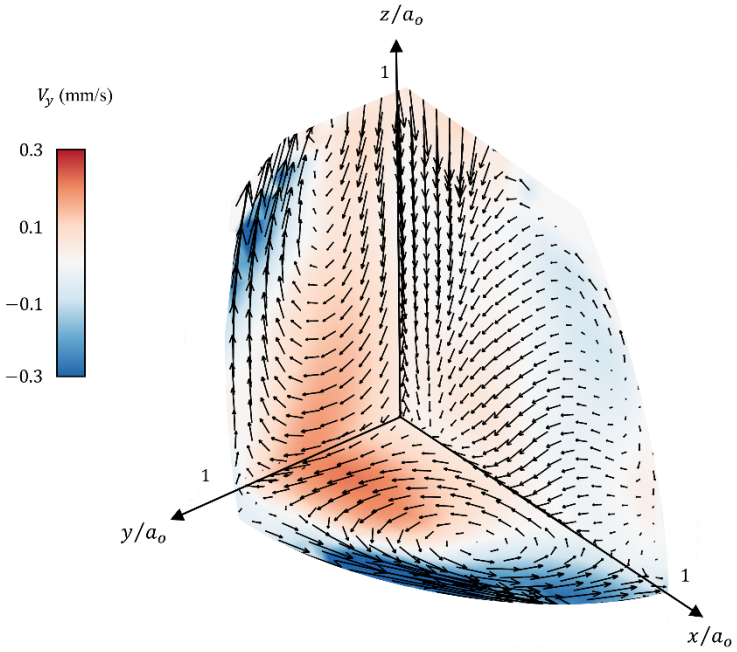

Figure 6: Three-dimensional velocity field in Eulerian referential for case III. For visualization purposes, 2D slices are shown at $x/a_o = y/a_o = z/a_o = 0$. A scalar field of the velocity component in the y-direction is also displayed.

We now analyze the three-dimensional structure of the vortices inside the drop. Vectors fields are shown in Fig. 7 for different values of z/a_o to highlight the effect of the depth of the drop in the vortical structures. A solid line is also added to illustrate the interface of the drop for visualization purposes. As it is clearly shown in the figure, the internal EHD flows evolve with z/a_o, being strongest at $z/a_o = 0$, as shown in Fig. 7 (a). As the slice position is shifted along the z-direction, both the area of the recirculation zone and the magnitude of the velocity vectors therein are smaller. At $z/a_o = 0.6$, where the vortices are firstly identified, the circulation is minimum. Although a direct comparison with the 2D trajectories shown in Fig. 2 is difficult due to the increased size and deformation of the drop, an overall similar flow structure is identified at $z/a_o = 0$. Note that only one half of the drop is shown for $0 < x/a_o < 1$ and $0 < y/a_o < 1$. However, a similar flow field is observed outside this region of the drop, whose measurements are not shown here for the sake of brevity.

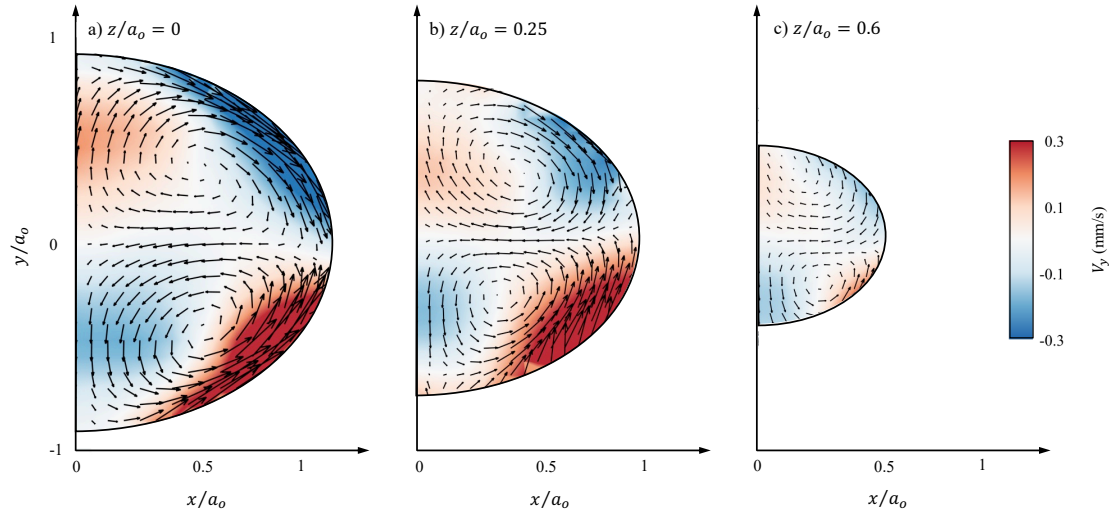

Figure 7: 2D slices $x - y$ plane of the velocity field in the for different positions in the z-direction, considering case III. Velocity vectors and the scalar field of V_y are shown.

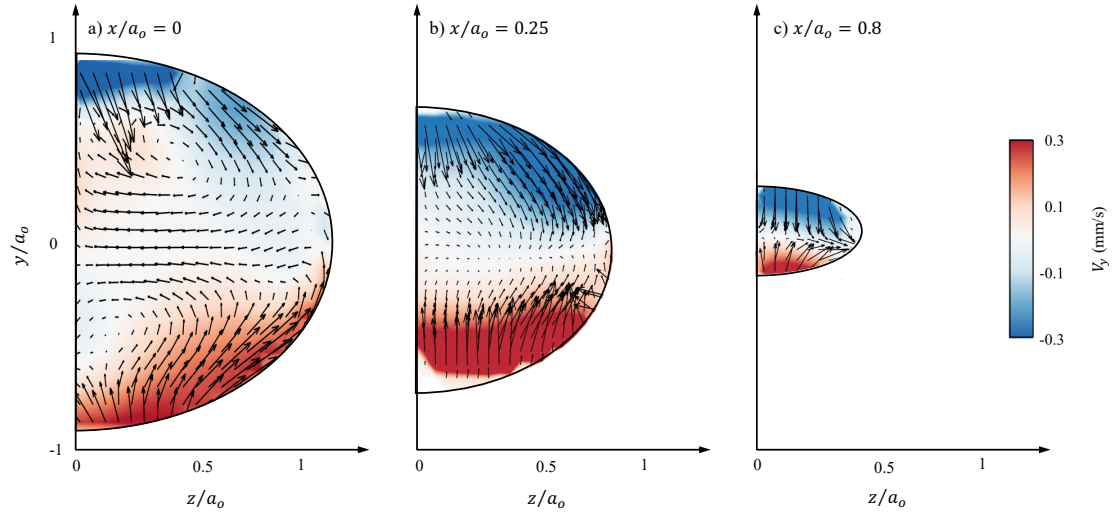

Figure 8: 2D slices $y - z$ plane of the velocity field in the for different positions in the x-direction, considering case III. Velocity vectors and the scalar field of V_y are shown.

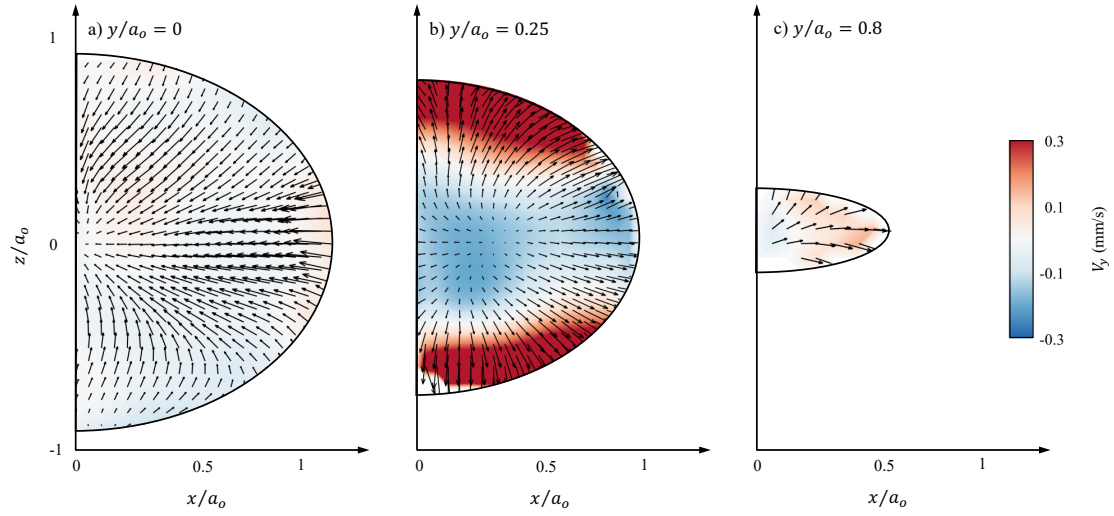

Figure 9: 2D slices $x - z$ plane of the velocity field in the for different positions in the y-direction, considering case III. Velocity vectors and the scalar field of V_y are shown.

Although a reasonably symmetrical flow field is seemingly observable along the z-direction, the necessity for accessing the three-dimensional structure of the EHD flows inside the drop becomes evident once the focus is shifted to other directions. As shown in Fig. 8, the flow structures evolve in a different way along the x-direction. Although some vorticity is observable when $x/a_o = 0$, as shown in Fig. 8 (a), the flow in the $y - z$ plane resembles a sink flow when $x/a_o = 0.25$ for which the internal circulation consists mainly in a radial component along the y-direction. This is even clearer close to the interface of the drop, as shown in Fig. 8 (b) ($x/a_o = 0.8$), where the tangential component is more evident. Interestingly, once we shift to the slices along the y-direction, an opposite behavior is noticed, as can be identified in Fig. 9 at the same corresponding positions of y/a_o in respect to the x-direction. Close to the interface ($y/a_o = 0.8$), the velocity is seemingly mostly due to its tangential component, with an outwards direction, as opposed to the slices along the x-direction. Closer towards the center of the drop, where $y/a_o = 0.25$, the V_y component is further developed, where the flow clearly resembles a source flow. Finally, at its plane of symmetry, when $y/a_o = 0$, as shown in Fig. 9 (a), the V_y velocity component is suppressed as can be identified from the scalar field, and the flow assumes mostly a planar configuration towards a stagnation point at $z/a_o = x/a_o = 0$. The structures here presented highlight the three-dimensional nature of the internal EHD flows of the drop.

4. Conclusions

This paper presented a novel methodology based on 2D and 3D Lagrangian Particle Tracking (LPT) algorithms to measure, for the first time, electrohydrodynamic (EHD) flows inside a neutrally buoyant leaky dielectric drop. Fluorescent particles are used as tracers, while an optical arrangement consisting of a monocavity laser, mirrors, cylindrical and spherical lenses was used to generate the laser sheet used for illumination. A thickness of around 150 μm was used for the 2D measurements at the plane of symmetry of the drop, while for the 3D measurements a thicker sheet with roughly 1 cm of thickness was used. The 3D positions and tracks of the particles were obtained using a multi-camera in-line arrangement exploiting the Scheimpflug principle and the polynomial camera model for volumetric calibration associated to a calibration refinement step.
By using two leaky dielectric liquids, namely Silicone and Castor oils, both the oblate and prolate drop configurations were investigated. For the 2D measurements, the strength of the electric field, E_o, was set at 0.50 and 0.30 kV/cm for cases I and II, respectively, so that the fluid system remains within the small-deformation limit ($Ca_E \ll 1$) for which the leaky dielectric model (LDM) is applicable. The 2D measurements of the velocity field at the plane of symmetry of drop the

revealed an excellent agreement with the LDM theory for both the oblate and prolate configurations. The internal flow structure consists of four-counter rotating vortices that retain its symmetry. The 3D measurements of the velocity field enable the analysis of the EHD flows in the whole bulk of the drop, considering a larger shape deformation, for which the profiles resemble the 2D structure when $z/a_o = 0$. However, the three-dimensional structure of the flow is clearly identified once the analysis is shifted along the other directions.

The proposed methodology offers thus valuable 2D and 3D measurements of the internal EHD flows of neutrally buoyant drop dispersed in a fluid with same density, covering both smaller and larger drop deformations. Dy doing so, it possible to extent the typical theoretical analysis offered by the LDM theory for a wider range of fluid systems as well extrapolating the plane of symmetry of the drop, which is particularly useful once the hypothesis of small deformations is no longer valid, for which the internal circulation is no longer expected to be symmetrical.

Acknowledgements

This project was financed by the Normandie region under the grant 22E05147.

References

Vlahovska, P. M. (2019). Electrohydrodynamics of drops and vesicles. In *Ann. Rev. Fluid Mech.* **51** (pp. 305-335).

Karp, J. R.; Lecordier, B.; Shadloo, M. S. (2024). Electrohydrodynamic flows inside a neutrally buoyant leaky dielectric drop. In *Phys. Fluids* **36** (053323).

Mikkelsen, A.; Khobaib, K.; Eriksen, F. K.; Maloy, K. J.; Rozynek, Z. (2018). Particle-covered drops in electric fields: Drop deformation and surface particle organization. In *Soft Matter* **14** (pp. 5442-5451).

Taylor, G. I. (1966). Studies in electrohydrodynamics I: The circulation produced in a drop by electric field. In *Proc. R. Soc. London* **291** (pp. 159-166).

Saville, D. A. (2003). The Taylor-Melcher leaky dielectric model. In *Ann. Rev. Fluid Mech.* **29** (pp. 27-64).

Taylor, G. I. (1969). Electrohydrodynamics: A review of the role of interfacial shear stresses. In *Ann. Rev. Fluid Mech.* **1** (pp. 111-157).

Torza, R. G.; Mason, S. G. (1971). Electrohydrodynamic deformation and burst of liquid drops. In *Proc. R. Soc. London* **269** (pp. 295-319).